ELECTRICAL AND CHEMICAL DOMAINS MAPS PROMOTED BY TiO_2 INCORPORATED IN A DLC MULTILAYER USING KELVIN PROBE FORCE MICROSCOPY (KPFM) AND CONFOCAL RAMAN ANALYSES

L. Vieira [1,2], T. B. Santos[1], L.O. Paula[1], L. Manfroi[1], P.A.Radi[1,2]

1 - University of Paraiba Valley, UNIVAP/ IP&D , São Jose dos Campos, SP, Brazil

2 - Technological Institute of Aeronautics, ITA/LPP, São Jose dos Campos, SP, Brazil

vieiral@ita.br

1. Introduction

Advances made in the controlled deposition of Diamond-like carbon thin films with varying morphologies have pushed researchers to consider DLC as an alternative carbon-based material for electronic devices[1;2]. DLC is a metastable form of amorphous carbon that contains a mixture of tetrahedral sp^3 and trigonal sp^2 carbon hybridizations. The sp^2 and sp^3 amounts in the films depend on the variation of parameters and deposition processes [2]. also buried nanoparticles are believed to be an effective approach to tune the physical, chemical and electrochemical properties of Diamond-like carbon films(DLC)[3].

Scanning capacitance microscopy (SCM) and electric force microscopy (EFM) based techniques have been used to investigate fundamental and applied research processes with a wide variety of applications [4,5]. Depending on the AFM setup, electrical force, surface potential and capacitance coupling ($\partial C/\partial z$) between tip and sample can be measured in a single pass. KPFM and the ($\partial C/\partial z$) measurements are carried out, by applying an AC voltage to the tip and monitoring the tip response at the AC frequency[6]. The key in KPFM technique is the Digital Analogic Controller (DAC) used to apply a direct Vdc voltage to the tip in order to minimize the oscillating force at frequency ω. This is obtained when the voltage Vdc has the same magnitude as the surface potential VCPD, leading to Fdc=Fω=0. Therefore, the local value of Vdc that minimizes Fω is a measurement of the difference in surface potential between the tip and the local studied surface[7].

Thus, the electric force in an EFM measurement can be written as a combination of three terms [12] :

$$F_{dc} = -\frac{1}{2}\frac{\partial C_{(z)}}{\partial z}\left[\frac{1}{2}(\mathbf{V_{dc}} - \mathrm{V_{CPD}})^2\right] \qquad (1)$$

$$F_{\omega} = -\frac{\partial C_{(z)}}{\partial z}(\mathbf{V_{dc}} - \mathrm{V_{CPD}})\,\mathbf{V_{ac}}\sin(\omega t) \qquad (2)$$

$$F_{2\omega} = \frac{1}{4}\frac{\partial C_{(z)}}{\partial z}\mathbf{Vac}^{\,2}[\cos(2\omega t) - 1] \qquad (3)$$

Where Vdc and Vac are the DC and the AC components of the potential applied to the tip, respectively, and V_{CPD} is the contact potential difference between tip and surface. The applied AC signal (Vac) creates oscillating electrostatic forces to the cantilever at frequencies ω and 2ω. Therefore, from equation 3 the electric force at frequency 2ω is directly proportional to ($\partial C/\partial z$). As described in the block diagram in Figure1, this signal is measured from amplitude output at lock-in #3. A tip moves in tapping mode over the surface and a laser reflected from the cantilever to a four quadrant-photo detector monitoring the tip deflection. The mechanical vibration of the tip close to its resonance is used to deduce the topography, normally by keeping the vibration amplitude constant and moving the z direction of the

piezo (first feedback loop over lock-in #1). Additional AC voltage with a much lower frequency is applied. This AC voltage gives rise to the two signal forces, as described by formulism above and reported in more details recently by some co-authors [8] .

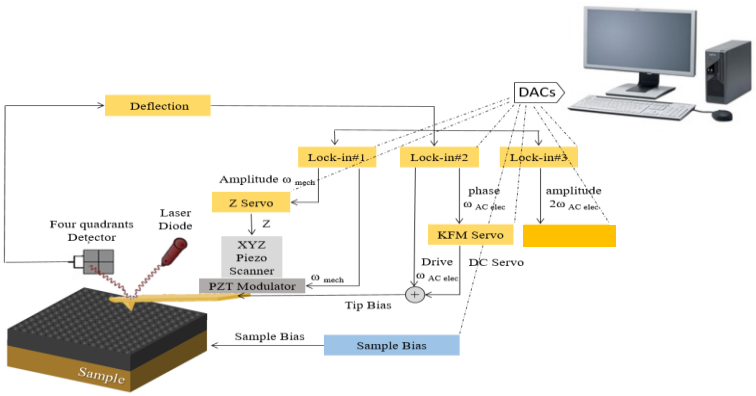

Figure 1: Block diagram during single pass scanning.

Buried nanostructures can be characterized by capacitance coupling ∂C/∂z, the authors of ref [9] investigate carbon nanotubes percolated inside a polymer matrix. Nevertheless, the surface is flat and the KPFM signal does not show any sign of the buried nanostructures. However, they are clearly identifiable in the ∂C/∂z image. In the same reference finite element based in modeling was carried out for direct information and access to the electrical properties of the buried nanostructures, and provides a physical model for the interaction of the carbon nanotubes with the surrounding matrix.

Although DLC can be deposited at low (<200 °C) substrate temperature it exhibits properties of graphite and also crystalline diamond. [10] . The combination of those properties are chemical inertness [11], optical transparency [12], high mechanical hardness [13], low friction coefficient [14], and very high electrical resistance [12], which together make DLC very attractive for use as a protective coating [14,15]. However, unmodified DLC films are electrically insulating, which prevents their application in several fields, including for electronics. Recently we reported a solution to overcome this problem using silver nanoparticles buried in DLC films. DLC-Ag is an attractive material for electronic devices. In addition, we measured electric carriers in DLC-Ag films after being scratched, which had improved potential in the trenches due to silver nanoparticles spread in the trenches [16].

2.0 Materials and Methods:

TiO_2:DLC production: DLC film with 0.5 µm of thickness was deposited by plasma enhanced chemical vapor deposition (PECVD) system model NPE-4000 from Nano-master. The plasma discharge was assisted by a load-locked parallel plate reactor using a Pinnacle Plus power supply from, Advanced Energy, and the operating parameters were controlled by computer. The film was deposited onto silicon (n-Si (100); $\rho < 0.004$ Ωcm) and substrates.

The deposition procedure was performed in two steps: plasma surface cleaning, and coating deposition. The precursor for DLC film was methane gas (CH_4). The following constant conditions were used in all steps: 7.0 Pa of working pressure, 200 W of power, 4.5µs pulse, and 100 KHz of frequency. The variable parameters were deposition time, temperature, and precursor mass flows as presented in an early article [17].

After DLC deposition, the DLC surface was treated with alcohol vapor, stirring TiO_2 in anatase nanoparticles phase, the vapor was produced in ultra sound under laminar flow. The TiO_2 were finally

anchored in the DLC matrix by an additional further thin DLC layer deposited over the TiO_2 nanoparticles. The final sample comprising layers of DLC and TiO_2 nanoparticles are show in figure 2.

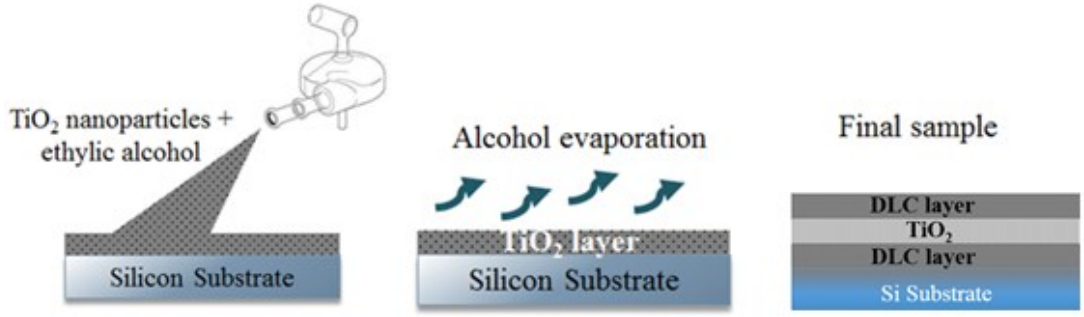

Figure 2 – Schematic process of TiO_2:DLC preparation

Raman spectroscopy: The atomic arrangement of the sp^2/sp^3 rate in DLC surface with and without TiO_2 anatase phase buried in DLC were analyzed by Raman scattering spectroscopy, using a Horiba LabRam HR Evolution system with an Ar^+ ion laser (λ = 514 nm), operated with backscattering geometry. The laser power on the sample was ~0.6 mW, and the diameter of the laser spot was 1.0 μm. The Raman shift was calibrated in relation to the diamond peak at 1332 cm^{-1}. All measurements were carried out in air at room temperature (294 k).

SPM measurement: A commercial Park NX 10 SPM instrument was used. This instrument has three internal lock-in, enabling the implementation of the $\partial C/\partial z$ as described in Figure 1.

Results and Discussion

The Ramam spectra results are presented in Figure 3, the plot has three spectra's: red line is a plot from standard TiO_2 anatase phase. Black line is a plot from standard DLC. Blue line is a plot from a mixture of TiO_2 in anatase phase and DLC. The blue plot was measure from a delimitated area of 45 μm^2 with TiO_2 cluster analyzed by Lab Spec 6 from Horiba System. The plots comparison show the presence of anatase phase in DLC film confirmed by micro-Raman which exhibited four Raman-active modes associated to anatase structure: A_{1g} (519 cm^{-1}), B_{1g} (397 cm^{-1}) and E_g (144 and 636 cm^{-1}) with a strong peak at 144 cm^{-1}. [18]. These Raman optical active modes and represents vibrations as stretching or bending as described in table I also these modes are sensitive with temperature. The measurement was run out at environment air under 294k. The anatase nanoparticles were sprayed in a DLC as described at section 2. For comparison a pure DLC signature is presented as indicated in previous literature, with two bands, namely, D band with sp^2 and sp^3 disordered bonds and G sp^2 graphite bonds centered at 1350cm^{-1} and 1580 cm^{-1} respectively plotted in green lines[21].

Comparing Raman spectra from DLC films with TiO_2:DLC films:, the TiO_2:DLC presents the D and G bands displacement towards left, of 32 cm^{-1} for D band and 46 cm^{-1} for G band. This Raman shift is indicative of the presence of carbon clusters in aromatic rings and chain. The chains are regions that may occur bonds or connections with existing oxygen in the film. This oxygen present in the film coming from the deposition process and also from the anatase phase. This results comproved the anatase phase in DLC films and compared anathase and DLC peaks in Raman spectra.

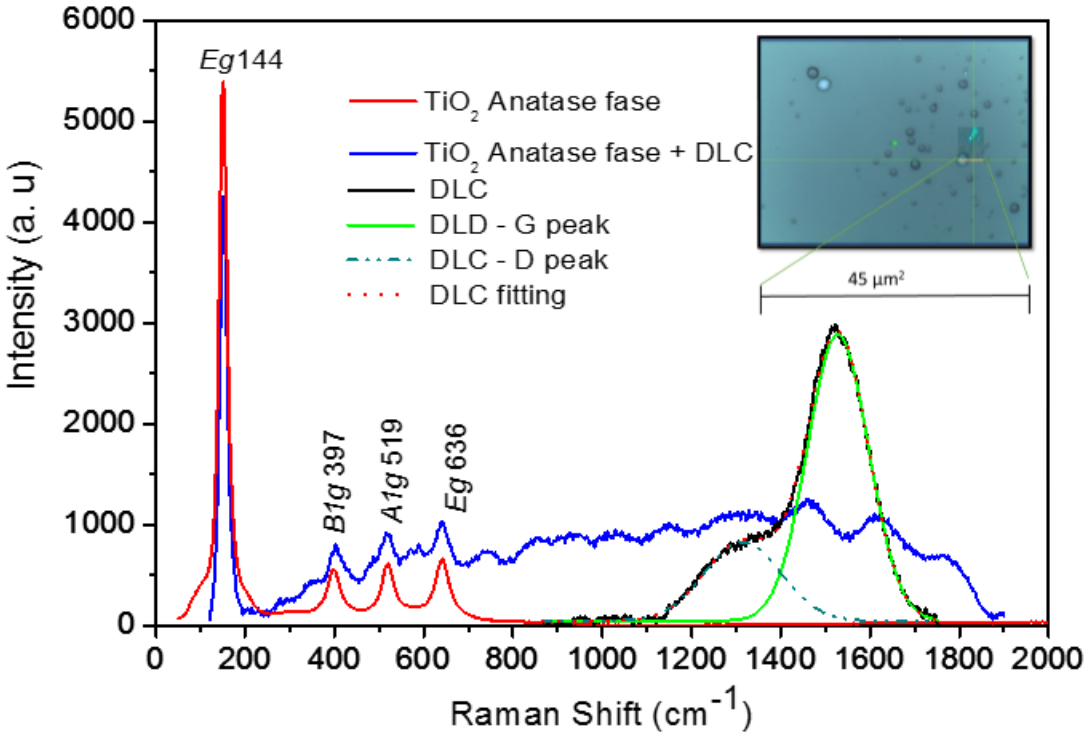

Figure 3 Raman spectroscopy plot comparison from the TiO_2 in anatase phase in red line, pure DLC film in black line and TiO_2:DLC in blue line .

The Raman-active frequencies and symmetry assignments using lasers in 514nm for the phonons in the anatase materials studied in this paper are summarized in TableI as described above. The experimental results using Ar^+ laser in (514-nm) were compared with literature[26] and same peaks where found with small displacements for Ti-O stretching vibration and and O-Ti-O bending vibration.

Table I- Raman active modes vibration comparison using Ar^+ laser in 514 nm for anatase phase[26].

Raman active modes vibration		O-O Stretching vibration Eg	Ti-O Stretching vibration B1g	Ti-O Stretching vibration And O-Ti-O Bending vibration A1g for 519cm^{-1} and Eg for 636 cm^{-1}	
		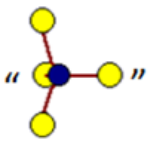	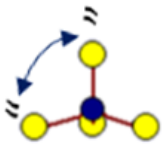	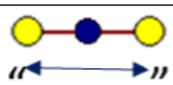	
Experimental results	Anatase	144 cm^{-1}	398cm^{-1}	514cm^{-1}	645cm^{-1}
Literature results	Anatase	144 cm^{-1}	397 cm^{-1}	519cm^{-1}	636cm^{-1}

Figure 4 shows the TiO_2:DLC images obtained on KPFM analysis implemented using the single pass. Three distinct information modes were split in three images related with: topography, surface potential and ∂C/∂z as explained in equations 1-3.

Figure 4(a) presents a topography image of the TiO_2:DLC film. A mix of DLC topography with TiO_2 clusters can be seen in this picture the total area presented roughness (rms) as 7nm. The height profile from Figure 4(a) was presented in Figure 4(d), from this profile was measured a cluster with 1.2 nm and also the profile roughness presented a mixture of DLC and anatase clusters that was identified by Raman analyses as TiO_2:DLC.

Figure 4 (b) shows the potential of surface from Figure 4(a). This image shows very low contrast between anatase phase buried and DLC. In another hand, Figure 4(c) shows ∂C/∂z image with higher contrast between anatase phase and DLC, where anatase phase presents lower ∂C/∂z compared with DLC region. Figure 4(f) shows the profiler from Figure 4(c) the profile presented a valley of 2 mV measured from cantilever deflection by AFM photodetector. The valley can be indicated as a region where positive ions were carried out, this area is sufficient to develop an electric dipole between TiO_2 anatase nanoparticles and DLC surfaces. Just to compare from literature important new results from carbon nanotubes phases buried in polymers was presented in Castaneda-Uribe and coworkers [16] they demonstrated depth sensitivity and spatial resolution of subsurface imaging of polymer nanocomposites using second harmonic mapping in Kelvin Probe Force. Recently Vieira L. and co-authors also published a KPFM study about silver nanoparticles spread in DLC after scratching tests. Best insulants materials has greater capacitance due to it the capacitance technique becomes very attractive to DLC with TiO_2 nanoparticles in anatase phase. TiO_2:DLC can be used as charge carriers.

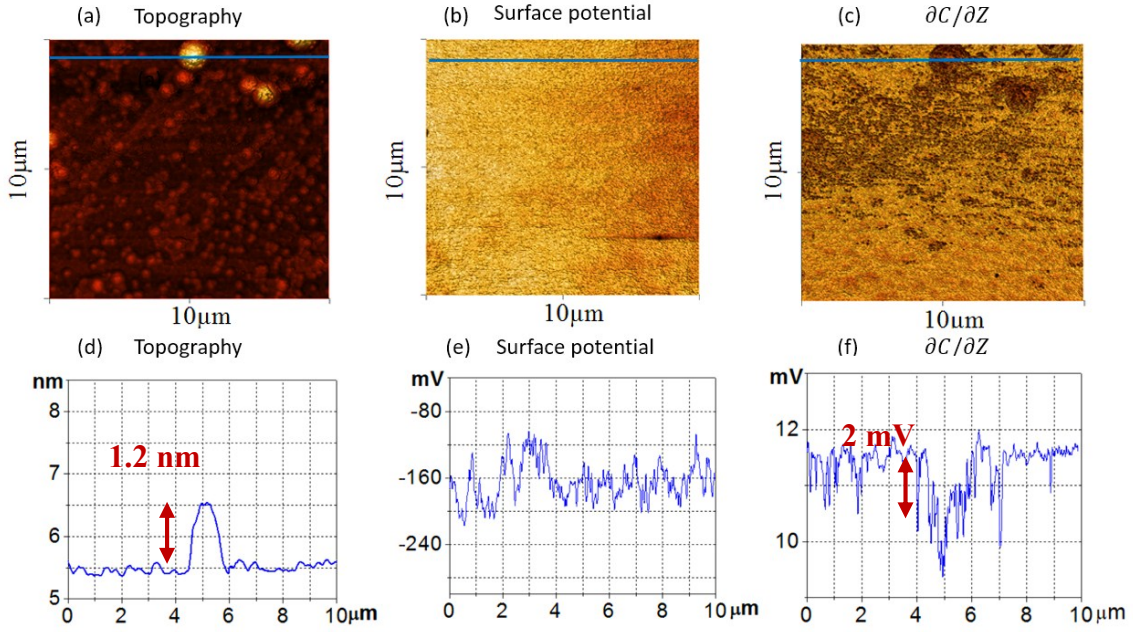

Figure 4 - Topography, surface potential, $\partial C/\partial Z$ images, and cross-section plots obtained on TiO_2:DLC.

Conclusions:

In this paper the Kelvin probe force microscopy (KPFM) was used to compare electric potential distribution on the surface of nanoparticles buried in amorphous carbon. The capacitance gradient ∂C/∂Z map associated with Raman analyses improved the possibility to observe the charges carriers from nanoparticles buried in amorphous carbon as demonstrated.

These chemical domains and surface potential distribution can be related with electron carries and electrical conductivity of TiO_2 in DLC films. These regions with electron carries can be used to evidence

areas to attach molecules or other substances that qualifying DLC + TiO_2 as unique materials with chemical, physical and electrical properties for a broad range of applications that include electronic and energy storage devices. The advantage offered by these materials is that their properties can be tuned by the control of TiO_2 nanoaparticles buried into DLC.

Acknowledgements

The authors are grateful for financial support received through CNPq project number 313280/2014-2 and FAPESP (Pronex) project number 11/50773-0 .

References

[1] Frackowiak E and Béguin F 2001 Carbon materials for the electrochemical storage of energy in capacitors *Carbon N. Y.* **39** 937–50

[2] Casiraghi C, Ferrari A C and Robertson J 2005 Raman spectroscopy of hydrogenated amorphous carbons *Phys. Rev. B* **72** 1–14

[3] Szunerits S and Boukherroub R 2013 Functionalization of diamond surfaces for medical applications *Diamond-Based Materials for Biomedical Applications* (Elsevier) pp 25–47

[4] Melitz W, Shen J, Kummel A C and Lee S 2011 Kelvin probe force microscopy and its application *Surf. Sci. Rep.* **66** 1–27

[5] Panchal V, Pearce R, Yakimova R, Tzalenchuk A and Kazakova O 2013 Standardization of surface potential measurements of graphene domains *Sci. Rep.* **3** 2597

[6] Cadena M J, Misiego R, Smith K C, Avila A, Pipes B, Reifenberger R and Raman A 2013 Sub-surface imaging of carbon nanotube–polymer composites using dynamic AFM methods *Nanotechnology* **24** 135706

[7] Nonnenmacher M, O'Boyle M P and Wickramasinghe H K 1991 Kelvin probe force microscopy *Appl. Phys. Lett.* **58** 2921–3

[8] Salomão F C, Lanzoni E M, Costa C A, Deneke C and Barros E B 2015 Determination of High-Frequency Dielectric Constant and Surface Potential of Graphene Oxide and Influence of Humidity by Kelvin Probe Force Microscopy *Langmuir* **31** 11339–43

[9] Castañeda-Uribe O A, Reifenberger R, Raman A and Avila A 2015 Depth-Sensitive Subsurface Imaging of Polymer Nanocomposites Using Second Harmonic Kelvin Probe Force Microscopy *ACS Nano* **9** 2938–47

[10] Casiraghi C, Robertson J and Ferrari A C 2007 Diamond-like carbon for data and beer storage Carbon is a very versatile element that can crystallize in the forms of **10** 44–53

[11] Chu P K and Li L 2006 Characterization of amorphous and nanocrystalline carbon films *Mater. Chem. Phys.* **96** 253–77

[12] Honglertkongsakul K, May P W and Paosawatyanyong B 2010 Electrical and optical properties of diamond-like carbon films deposited by pulsed laser ablation *Diam. Relat. Mater.* **19** 999–1002

[13] Fernandes J V, Antunes J M, Cavaleiro A, Menezes L F and Simoes M I 2002 Ultra-microhardness testing procedure with Vickers indenter **149** 27–35

[14] Radi P A, Santos L V, Bonetti L F, Rodrigues G C and Trava-Airoldi V J 2008 Friction and wear maps of titanium alloy against a-C:H20% (DLC) film *Surf. Coatings Technol.* **203** 741–4

[15] Heimberg J a., Wahl K J, Singer I L and Erdemir a. 2001 Superlow friction behavior of diamond-like carbon coatings: Time and speed effects *Appl. Phys. Lett.* **78** 2449

[16] Vieira L, Lucas F L C, Fisssmer S F, dos Santos L C D, Massi M, Leite P M S C M, Costa C A R, Lanzoni E M, Pessoa R S and Maciel H S 2014 Scratch testing for micro- and nanoscale evaluation of tribocharging in DLC films containing silver nanoparticles using AFM and KPFM techniques *Surf. Coatings Technol.* **260** 205–13

[17] Radi P A, Marciano F R, Lima-Oliveira D A, Santos L V, Corat E J and Trava-Airoldi V J 2011 Influence of crystalline diamond nanoparticles on diamond-like carbon friction behavior *Appl. Surf. Sci.* **257** 7387–93

[18] Ohsaka T, Izumi F and Fujiki Y 1978 Raman spectrum of anatase, TiO2 *J. Raman Spectrosc.* **7** 321–4

[19] Swamy V, Muddle B C and Dai Q 2006 Size-dependent modifications of the Raman spectrum of rutile TiO[sub 2] *Appl. Phys. Lett.* **89** 163118

[20] Ohsaka T, Yamaoka S and Shimomura O 1979 Effect of hydrostatic pressure on the Raman spectrum of anatase (TiO2) *Solid State Commun.* **30** 345–7

[21] Robertson J 2002 Diamond-like amorphous carbon *Mater. Sci. Eng. R Reports* **37** 129–281